Science of the Total Environment 653 (2019) 1192–1203

Contents lists available at ScienceDirect

Science of the Total Environment

journal homepage: www.elsevier.com/locate/scitotenv

Evidences of copper nanoparticle exposure in indoor environments: Long-term assessment, high-resolution field emission scanning electron microscopy evaluation, in silico respiratory dosimetry study and possible health implications

Maurizio Manigrasso [a,*], Carmela Protano [b], Maria Luisa Astolfi [c], Lorenzo Massimi [c], Pasquale Avino [d], Matteo Vitali [b], Silvia Canepari [c]

[a] Department of Technological Innovations, INAIL, Via IV Novembre 144, 00187 Rome, Italy
[b] Department of Public Health and Infectious Diseases, Sapienza University of Rome, P.le Aldo Moro 5, 00185 Rome, Italy
[c] Department of Chemistry, Sapienza University, P.le Aldo Moro 5, I-00185 Rome, Italy
[d] Department of Agricultural, Environmental and Food Sciences (DiAAA), University of Molise, via De Sanctis, I-86100 Campobasso, Italy

HIGHLIGHTS

- Appliances operated by brush electric motors emit Cu nanoparticles (NPs).
- 10^6–10^7 NPs deposit on the olfactory bulb during appliances operation (1.5–6 min).
- Both single 20–40 nm NPs and aggregated particles were observed through HR-FESEM.
- Cu indoor contamination was >2-fold higher indoor than outdoor.
- General population is chronically exposed to Cu NPs in indoor environments.

GRAPHICAL ABSTRACT

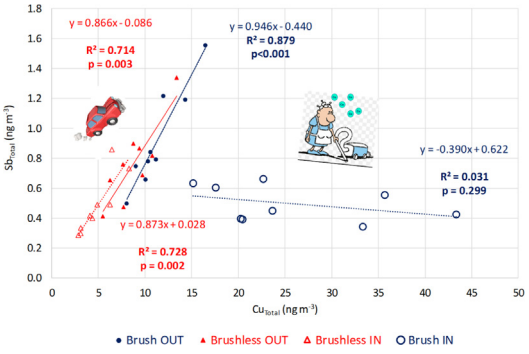

ARTICLE INFO

Article history:
Received 21 September 2018
Received in revised form 2 November 2018
Accepted 3 November 2018
Available online 06 November 2018

Editor: Jay Gan

Keywords:
Indoor copper nanoparticles
Brush electric motors
Chronic exposure
Olfactory bulb
Multiple-path particle dosimetry model
High-resolution field emission scanning electron microscopy

ABSTRACT

A variety of appliances operated by brush electric motors, widely used in indoor environments, emit nanoparticles (NPs). Due to electric arc discharge during the operation of such motors, some NPs contain copper (Cu). Their dimensions are the same of those found in brain tissue samples by other authors who speculated their possible translocation to brain through olfactory bulb. Cu has been reported to play an important role in the etiopathogenesis of Alzheimer's disease. Thus, the present study was performed to 1. estimate by means of Multiple-Path Particle Dosimetry model the doses of NPs released by electric appliances that can potentially deposit on the olfactory bulb; 2. investigate the morphology and the composition of particles emitted by some electric appliances daily used in indoor environments; 3. monitor for a long time period the Cu contamination of indoor environments due to this kind of appliances. About 10^6–10^7 NPs deposit on the olfactory bulb during the operation (1.5–6 min) of such appliances, with a major contribution due to 10–20 nm NPs. HR-FESEM characterization confirmed the presence of such NPs, that were observed both as individual particles (20–40 nm) and aggregated to form particles in the μm sizes range. XEDS microanalysis revealed the presence of Cu together with other elements. Relevant daily contamination of indoor environments due to these appliances has been confirmed by monitoring throughout a year the Cu content of PM_{10} samples collected both indoor and outdoor

* Corresponding author.
E-mail address: m.manigrasso@inail.it (M. Manigrasso).

https://doi.org/10.1016/j.scitotenv.2018.11.044

private dwellings. Cu was present in great part as an insoluble form. This means that, following protracted exposure, Cu NPs of such origin may undergo tissue accumulation. This is cause of concern because general population is chronically exposed to such Cu nanoparticles in indoor environments and in view of the role assigned to Cu in the development of neurological disorders.

1. Introduction

Air pollution remains an issue of great concern for public health, and it is one of the major risk factors for environmental and human health worldwide. The update 2018 of the World Health Organization Global Ambient Air Quality Database reported that, globally, seven million deaths were attributable to the joint effects of ambient and household air pollution (WHO, 2018). Indeed, over the years, air pollution was associated to a great number of adverse outcomes for human health, following both acute and chronic exposure. In particular, several evidences linked air pollution exposure to adverse health effects, such as respiratory (asthma, chronic obstructive pulmonary disease) and cardiovascular diseases (myocardial infarction, heart failure, cerebrovascular accidents) (Mannucci et al., 2015), endocrine disorders (Darbre, 2018), neuroinflammation and neurodegenerative diseases (Levesque et al., 2011). Outdoor air pollution was recently recognized as IARC Group 1, carcinogenic to humans (IARC, 2013). Besides, air pollution has been related to several adverse outcomes during intrauterine development (Burris and Baccarelli, 2017; Westergaard et al., 2017; Veleminsky Jr. et al., 2016).

Despite the increasing growth of scientific evidence on negative outcomes related to air pollution exposure, many gaps in this field still wait to be filled. First of all, it is well-known that air pollution is a complex mixture; thus, it is important to understand which components are the most dangerous for human health. Over the years, many researchers focalized the attention on Particular Matter (PM), especially on fine particles (<2500 nm diameter), and nanoparticles (NPs; <100 nm diameter). Indeed, independently from its chemical composition, PM has been linked to numerous human health adverse effects affecting respiratory, cardiovascular, endocrine and neurological systems (Anderson et al., 2012; Noh et al., 2016; Wang et al., 2017). In particular, NPs seem to play an important role on the health threats related to PM exposure (Hoek et al., 2010) because the small size of these particles allows them to persist for longer times, to easily contaminate indoor environments (Brauer et al., 1989) and/or to be transported over long ranges. Their high surface area, confer them an increased ability to adsorb organic molecules. Moreover, their size is smaller than those of cellular structures, so that they can penetrate into cellular targets in the lung and systemic circulation (Li et al., 2003; Pagano et al., 1996). Another important issue on air pollution is related to the contribution of outdoor and indoor air quality on human health. Traditionally, the attention of the scientific community was focused on outdoor air pollution, but in the last decades, indoor air quality has become increasingly important for two main reasons: 1. people spend a great part of their time in enclosed environments (>90%) (Hubal et al., 2000; CalEPA, 2004); 2. the quality of indoor air may be worse than outdoor, because indoor air contaminants not only derive from the outdoor pollutants, but are also produced directly indoor (Morawska et al., 2017; Śmiełowska et al., 2017). As regards to the indoor sources of air pollutants, several combustion activities (tobacco smoking, cooking activities, burning mosquito coils, burning incense and candles, traditional and alternative heating systems such as biomass-burning heating) represent well-known particles sources in indoor environments (Sarwar et al., 2004; Hsu et al., 2012; Huang et al., 2012; Liu et al., 2014; Protano et al., 2016; Protano et al., 2017; Stabile et al., 2018, Frasca et al., 2018; Drago et al., 2018). More recently, some studies demonstrated that the use of several non-combustion sources (drills, flat irons, hair dryers, laser printer, electronic smoking devices, etc.) contribute to the PM indoor pollution, increasing significantly the levels of indoor ultrafine- and NPs (Castellano et al., 2012; Manigrasso et al., 2017; Scungio et al., 2017).

Within this context, in previous studies (Manigrasso et al., 2017; Manigrasso et al. 2018) we addressed that potential sources present in domestic environments determine very intense exposure patterns to NPs. In particular, we observed that a fraction of NPs with mode of about 10 nm is present in the aerosol emitted by appliances operated by brush electric motors. This fraction is of great concern for human health for its size range. Indeed, anthropogenic particles of similar size were recovered in brain samples by other researchers, that hypothesized that such particles may bypass the typical way of uptake (circulatory system, blood-brain barrier) and reach the brain directly through the olfactory bulb (Maher et al., 2016). This fraction is cause of concern also due to its chemical composition. It contains copper NPs and copper ions have been reported to play an important role in the etiopathogenesis of Alzheimer's disease (AD) (Huang et al., 1999a, 1999b; Tabner et al., 2011).

Following our previous findings, the aims of this study are as follows:

1. to estimate the doses of NPs that can potentially deposit on the olfactory bulb, because they are candidate to possibly translocate to the brain;
2. to investigate the morphology and the composition of particles emitted by some electric appliances daily (or even several time a day) used in indoor environments, because their possible health effects derive from the association of their size and their chemical composition (Cu content);
3. to monitor for a long time period the Cu contamination of indoor environments due to this kind of appliances, in order to assess the time-exposure pattern of the general population.

2. Materials and methods

Aerosol measurements were performed both in a test-room and in real scenario indoor environments.

Aerosol number size distributions were measured in the test-room and were used to estimate the dose of particle deposited on the olfactory bulb. In the same room aerosol samples were collected for High-Resolution Field Emission Scanning Electron Microscopy (HR-FESEM) characterization.

In the real scenario environments PM_{10} samples were collected throughout a year to determine airborne concentrations of Cu and Antimony (Sb, as a tracer of vehicular traffic).

2.1. Test-room aerosol measurements and sampling

Aerosol was released during the operation (about 5 min) of a brush electric motor vacuum cleaner, an electric drill and a hairdryer in a test room. A detailed aerosol characterization is reported in a previous study (Manigrasso et al., 2017). Briefly, aerosol measurements were carried out in a 52.7 m^3 room where the door and window were both closed. During the aerosol measurements, the room temperature and relative humidity ranged between 24 °C and 26 °C and 25% and 32%, respectively. The air exchange rate (λ), calculated using the tracer gas technique (Laussmann and Helm, 2011), was equal to 0.67 h^{-1}.

Due to the fast evolution of the aerosol studied (Manigrasso and Avino, 2012; Manigrasso et al., 2013), aerosol number size distributions were measured by means of a Fast Mobility Particle Sizer (FMPS, model 3091, TSI, Shoreview, MN, USA). The instrument counts and classifies particles according to their electrical mobility in 32 size channels ranging from 5.6 to 560 nm with a 1 s time resolution. FMPS operates at a high flow rate (10 L min^{-1}) to minimize diffusion losses. It operates at ambient pressure to prevent the evaporation of volatile and semivolatile particles (TSI Particle Technology, 2015).

In the same test-room, for each appliance studied, aerosol samples for HR-FESEM characterization were collected on polycarbonate filters (0.8 μm, 47 mm, Sterlitech Corporation, WA, USA) at a sampling flow rate of 20 L min^{-1}. Before each sampling, air was completely changed and a blank sample was collected.

2.1.1. Aerosol dosimetry

The fractions of particles deposited on the olfactory bulb upon inhalation ($F^{Olf}(d_i)$) have been estimated using the Multiple-Path Particle Dosimetry model (MPPD v3.01, ARA 2015, ARA, Arlington, VA, USA) (Asgharian et al., 2001). For this estimate, MPPD relies on the study of Garcia et al. (2015). To estimate the dose of particles deposited in the head region, the 60th percentile human stochastic lung was considered along with the following settings: (i) a uniformly expanding flow, (ii) an upright body orientation, and (iii) nasal breathing with a 0.5 inspiratory fraction and no pause fraction. Moreover, the following parameters were used for a Caucasian adult male under light work physical activity, based on the ICRP report (ICRP, 1994): (i) a functional residual capacity (FRC) of 3300 mL, (ii) an upper respiratory tract (URT) volume equal to 50 mL, (iii) a 20 min^{-1} breathing frequency, and (iv) an air volume inhaled during a single breath (tidal volume, V_t) of 1.25 L.

Since FMPS measures aerosol size number distribution as a function of the electrical mobility diameter (d), d values have been transformed to aerodynamic diameter (d_a) according to Eq. (1) (X. Li et al., 2016).

$$d_a = d\sqrt{\chi \times \frac{\rho \times C_c(d_m)}{C_c(d_a)}} \tag{1}$$

where C_c is the Cunningham slip factor for a given diameter, χ is the particle dynamic shape factor ($\chi = 1$, i.e. spherical particles have been assumed), and ρ is the particle density. Particles with electrical mobility diameters from 6.4 to 14.3 have been considered as due to the emissions from the copper windings in the rotor whereas particles from 16.5 to 25.5 have been considered to arise from graphite electrodes (Bau et al., 2010) in the stator of the electric motor. The relevant particle densities as functions of particle mobility diameters have been calculated using the equations derived by Charvet et al. (2014).

For each respiratory act, the doses below described were calculated:

Size number dose distributions of particles deposited on the olfactory bulb upon inhalation as function of time (t):

$$D^{Olf}(d_i, t) = F^{Olf}(d_i) \times C(d_i, t) \times V_t \tag{2}$$

where d_i is the diameter of particles classified in the ith FMPS size channel, $F^{Olf}(d_i)$ is the relevant olfactory bulb deposition fraction, $C(d_i,t)$ is the concentration of particles in the ith FMPS size channel as a function of time, V_t is the tidal volume.

Cumulative size number dose distribution and cumulative number doses were calculated over the time interval of source operation (from t_0 to t_s) according to Eqs. (3) and (4), respectively.

$$D_c^{Olf}(d_i, t_s) = \sum_{t=t_0}^{t_s} D^{Olf}(d_i, t) \tag{3}$$

$$D_c^{Olf}(t_s) = \sum_{1=1}^{32} D_c^{Olf}(d_i, t_s) \tag{4}$$

where 32 is the number of FMPS size classes.

The surface area doses $S^{Olf}(d_i,t)$, $S_C^{Olf}(d_i,t_s)$, $S_C^{Olf}(t_s)$, were calculated from $D^{Olf}(d_i,t)$, $D_C^{Olf}(d_i,t_s)$, $D_C^{Olf}(t_s)$ under the hypothesis of spherical particles.

Background respiratory doses $D_C^{Olf}(d_i,t_s)$ and $S_C^{Olf}(d_i,t_s)$ have been calculated using the particle size number distributions averaged over 5 min time interval, before the operation of each indoor source considered.

2.1.2. Scanning electron microscopy characterization

A HR-FESEM (model AURIGA; Carl Zeiss Microscopy GmbH, Jena, Germany) equipped with an energy dispersive spectrometer for X-ray microanalysis (XEDS, model QUANTAX; Bruker Italia S.r.l., MI, Italy) was used for individual particle characterization of Cu.

A small portion of sample (about a quarter of total filter area) was cut in the center of polycarbonate membranes and coated with an ultra-thin gold layer (5 nm) by sputtering machine (Q150T Turbo-Pumped Sputter Coater/Carbon Coater; Quorum Technologies Ltd., East Sussex, United Kingdom).

HR-FESEM XEDS acquisitions were performed under high vacuum (10^{-6} hPa) at 20 keV accelerating voltage. Micrographs were acquired by Secondary Electron Detector (SED) at magnification, Working Distance (WD), tilt angle, and spot size conditions properly adjusted on a case-sensitive scale to optimize image resolution.

The microanalysis was performed at WD and magnification ranging from 9.6 mm to 12.4 mm and from 25,000× to 600,000×, respectively.

2.2. Real scenario indoor aerosol sampling

Samplings were performed in two dwellings located in the Terni basin (Central Italy), an area characterized by quite intensive urban and industrial PM emissions (Massimi et al., 2017; Fig. 1). The dwellings were both located at the first floor and at short distance from the industrial area (steel plant): the first one (DW1) was in close proximity (about 20 m) to a trafficked urban road; the second one (DW2) was at about 150 m from a secondary road. Samplings were performed by low cost samplers (High Spatial Resolution Samplers; HSRS, recently made available from Fai Instrument S.r.l., Fonte Nuova, Rome, Italy), equipped with a PM_{10} sampling head. These samplers are very silent and work at a very low flow rate (0.5 L min^{-1}). Thus they enable to accumulate PM on membrane filters for long times (one month or more), ensuring a high representativeness of the measured concentrations without excessive costs.

At each dwelling two samplers were placed: one indoor (in the dining room, at about 2 m from the window) and one in the outdoor environment at about 8 m from the dining room window. Both dining rooms were naturally ventilated, South-exposed and both kitchens were separated from the dining room and equipped with a methane stove and with an exhaust system. At each site, PM_{10} was sampled on a Teflon® membrane (37 mm diameter, 2 μm pore size, PALL Corporation, Port Washington, New York, NY, USA) at the same time. The monitoring activities lasted for about one year and the sampling periods are reported in Table 1.

In the first dwelling (DW1) a vacuum cleaner equipped with a bag filter and a 1300 W brush electric motor (the same used for aerosol measurements in the test-room) was used; no other appliance operated by this kind of electric motors was ever used. In the second dwelling (DW2) the floor cleaning was carried out by means of a vacuum cleaner equipped with a HEPA filter (class H11) and a 900 W brushless electric motor. This kind of motors is more efficient than brush electric ones, does not generate sparks, and consequently does not emit aerosol, as brush motors do. This is confirmed by Fig. 2 were the aerosol emissions measured in the test room of the two vacuum cleaners is compared. In

Fig. 1. Geographical location of sampling sites (QGis 2.18 Las Palmas). Legend - violet: industrial areas; red: urban areas; grey: agricultural areas; yellow: semi-natural areas; green: forests (Corine Land Cover 2012). (For interpretation of the references to colour in this figure legend, the reader is referred to the web version of this article.)

particular, the temporal trends of particle number concentrations in the range 5.6–560 nm measured close to the breathing zone of the user are shown.

2.2.1. Chemical analysis

PM_{10} mass concentration was gravimetrically determined by weighting Teflon® filters before and after sampling (Sartorius AG mod. ME5, Goettingen, Germany; 1 μg sensitivity). All the filters were conditioned at 50% R.H. and 20 °C for 48 h before each weighing step. After sampling, filters were sealed in plastic Petri dishes and stored at 5 °C until the chemical analysis.

A detailed description of the analytical procedure is reported in Canepari et al. (2006a, 2006b, 2010a). Briefly, sampled Teflon® membrane was deprived of the supporting polymethylpentene ring and subjected to ultrasound-assisted extraction (30 min; 40 kHz, 240 W; Ulsonic Proclean 10.0; Zielona Gora, Poland) in 20 mL of ultra-pure deionized water (Elga LabWater Purelab Plus, Wycombe, United Kingdom). The solution was then filtered on nitrate cellulose (NC) filters (porosity 0.45 μm, Millipore, Billerica, Massachusetts, USA) to obtain the soluble fraction. The insoluble particles on the NC and Teflon® filters were digested in microwave oven (quartz vessels; Ethos 1 Touch Control, Milestone, USA) by 3 mL of 2:1 concentrated HNO_3/H_2O_2 mixture (Promochem, LGC Standards GmbH, Wesel, Germany). The obtained solution was diluted to 50 mL with ultrapure water and again filtered, by using disposable syringe (Einmalspritzen Luer 20 mL, Sandtler) equipped with NC fiber filter (0.45 μm porosity, GVS Filter Technology – Indianapolis, USA), to obtain the residual fraction.

Both the soluble and insoluble fractions were analyzed by Inductively Coupled Plasma Mass Spectrometry (ICP-MS; Bruker 820 MS, Bremen, Germany, equipped with a glass nebulizer working at 0.4 mL min^{-1} - MicroMist™; Analytik Jena AG, Jena, Germany). Five-point matrix-matched calibration was used for the quantification of ^{65}Cu and ^{121}Sb; ^{89}Y was used as internal standard. An exhaustive description of ICP-MS operative conditions is reported in Astolfi et al. (2018).

Table 1
Sampling periods at dwellings 1 and 2.

Start	Stop	Name of period
January, 21st, 2017	February, 20th, 2017	Feb
February, 25th, 2017	March, 27th, 2017	Mar
April, 1st, 2017	May, 1st, 2017	Apr
May, 6th, 2017	June 5th, 2017	May
June, 10th, 2017	July, 17th, 2017	Jul
July, 22nd, 2017	August, 28th, 2017	Aug
September, 2nd, 2017	October, 2nd 2017	Sep
October 21st, 2017	November, 20th, 2017	Nov
November, 25th, 2017	January, 15th, 2018	Dec

2.3. Quality assurance

Before the measuring campaign, the performances of FMPS were checked by comparison with a Scanning Mobility Particle Sizer (SMPS, model 3936, TSI) equipped with an Electrostatic Classifier (model 3080, TSI), a Differential Mobility Analyser (DMA, model 3081, TSI) and a Condensation Particle Counter (model 3775, TSI). The FMPS number concentrations were approximately 15% lower than the diffusion loss corrected SMPS number concentrations, in agreement with the findings of Jeong and Evans (2009).

The performances of HSR Samplers were evaluated in terms of efficiency and repeatability (Perrino et al., paper in preparation). The repeatability of PM_{10} mass concentration measurements performed by HSRS (nine samplings, three replicates each) was acceptable, with relative standard deviation (RSD%) ranging from 2% to 25%. These values are probably mostly affected by the alteration of solid-vapor equilibria of

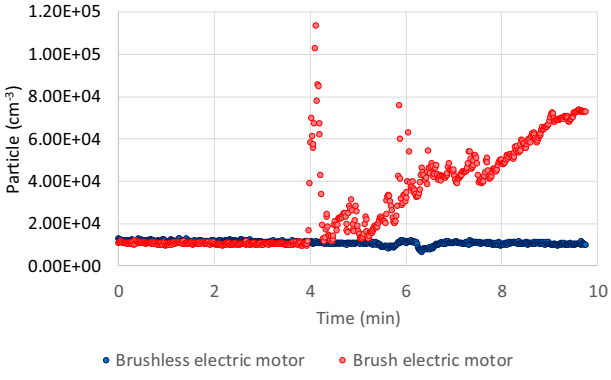

Fig. 2. Temporal trends of particle number concentrations in the range 5.6–560 nm measured for two vacuum cleaner equipped respectively with a brush and a brushless electric motor (respectively used at DW1 and DW2). The two vacuum cleaners were turned-off for the first 4 min.

volatile species, such as NH_4NO_3, during the prolonged HSRS sampling period. Very good repeatability (RSD% ranging from 6 to 15%, which includes contributes from chemical analysis) was obtained for stable elements, such as Cu and Sb.

The analytical procedure applied to the PM_{10} samples for the determination of elemental concentrations was previously fully validated (Canepari et al., 2006b, 2009). Cu and Sb were recovered from certificate material NIST1648 (urban dust) with recovery percentages higher than 90% and repeatability on field PM_{10} paired samples was very good, with RSD% lower than 10%.

2.4. Statistical elaboration

Statistical analyses were performed using IBM-SPSS version 25.0 software (IBM Corp. Released 2017. IBM SPSS Statistics for Windows, Version 25.0. Armonk, NY: IBM Corp.). Firstly, the Kolmogorov–Smirnov test was used to assess the normality of the distribution both for particles number concentrations and for Cu, Sb and PM_{10} levels. Particles number concentrations exhibited a not normal distribution; thus non-parametric tests were used for statistical evaluations. In particular, Mann-Whitney *U* test was used for assessing differences in median levels of the $D^{Olf}(d_i,t)$ for each particle diameter measured respectively before and during the period of each appliance operation. We considered particle diameters from 5.6 to 93 nm because above such size range, the particle deposition fraction $F^{Olf}(d_i)$ was negligible. Cu, Sb and PM_{10} levels were normally distributed; therefore, statistical elaborations were performed via parametric techniques. In particular, t-Student test for paired data was used to compare differences in mean levels of Cu, Sb and PM_{10} found indoor and outdoor, independently considering DW1 and DW2 sites. Besides, simple regression analyses were run to assess the relationship between Cu and Sb levels, separately for DW1 indoor, DW1 outdoor, DW2 indoor and DW2 outdoor concentrations. Finally, ANOVA test with Bonferroni post-hoc tests were used to assess the differences in the percentages of indoor and outdoor Cu soluble fractions for DW1 and DW2 sites.

3. Results and discussion

3.1. Dosimetry

Fig. 3a–c describe the particle number dose size distributions $D^{Olf}(d, t)$ of the particles deposited on the olfactory bulb, for each respiratory act, upon inhalation, during and after the operation of a brush electric motor vacuum cleaner, a hairdryer and an electric drill.

For these appliances, a major mode was present at about 10 nm, due to the Cu NPs emitted by the electric arc discharge between the Cu windings and the graphite electrodes of the brush electric motor (Manigrasso et al., 2015, Manigrasso et al., 2017; Szymczak et al., 2007). A minor mode at about 16 nm and, for the hairdryer and the vacuum cleaner, a shoulder at about 29 nm were probably due to particle coagulation and/or to the contribution from the graphite brushes (Roth et al., 2004). Following a single respiratory act, due to aerosol spike emissions, up to 7.6×10^4, 1.7×10^5 and 3.3×10^5 particles were respectively deposited on the olfactory bulb, with a major contribution, respectively of 1.3×10^4, 2.7×10^4 and 6.2×10^4 particles, from 9 to 10 nm particles. Throughout the time interval of appliance operation

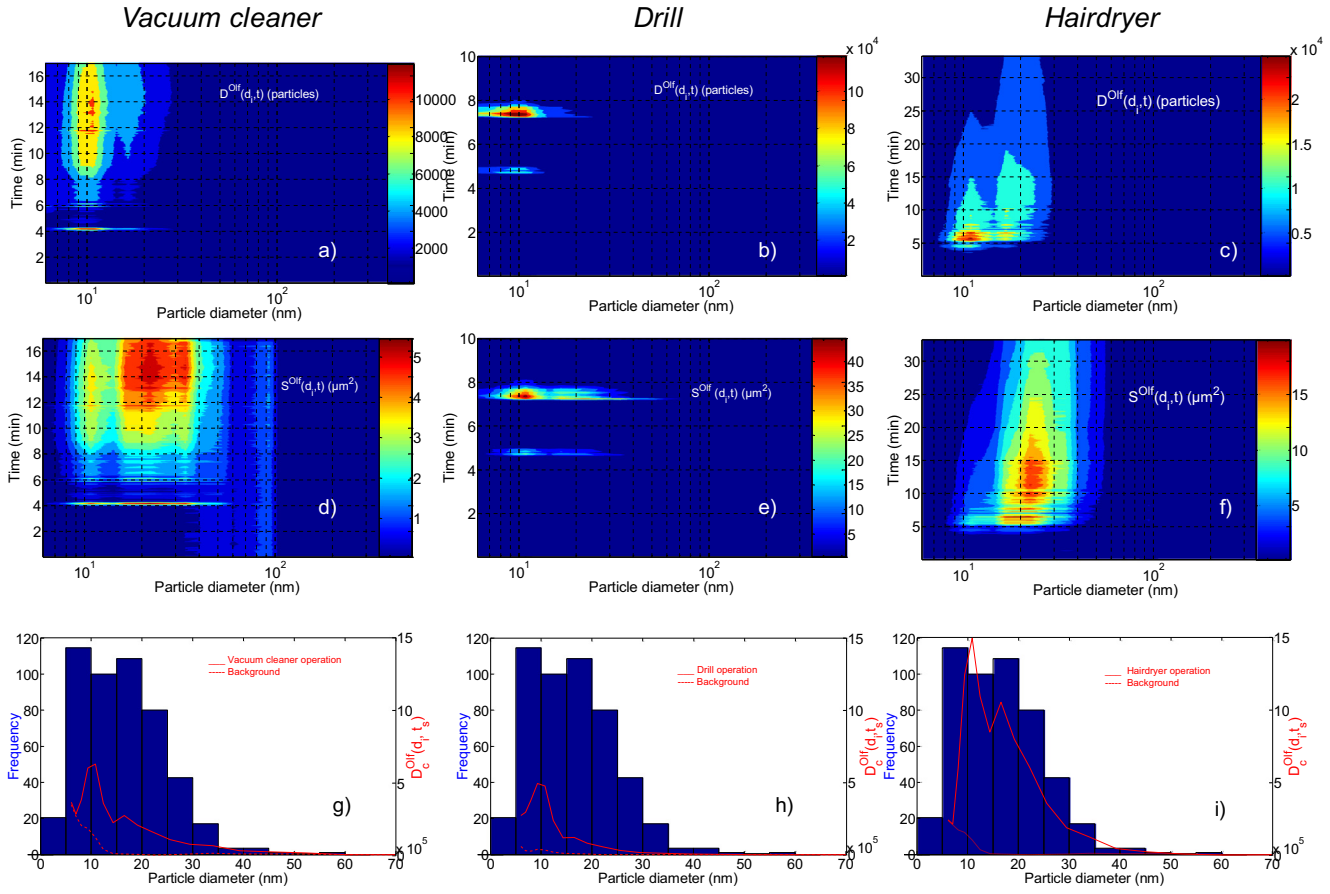

Fig. 3. a–c: Size number dose distributions $D^{Olf}(d_i,t)$. d–f: size surface area dose distributions $S^{Olf}(d_i,t)$. g–i: cumulative size number dose distribution $D_c^{Olf}(d_i,t_s)$ of particles deposited on the olfactory bulb upon inhalation following the operation for t_s min of a brush electric motor vacuum cleaner ($t_s = 6$ min) an electric drill ($t_s = 1.5$ min) and a hairdryer ($t_s = 5$ min) compared with the average value of the frequencies of the magnetite NPs retrieved by Maher et al. (2016) in brain tissue samples, as a function of the longest and of the shortest particle diameters.

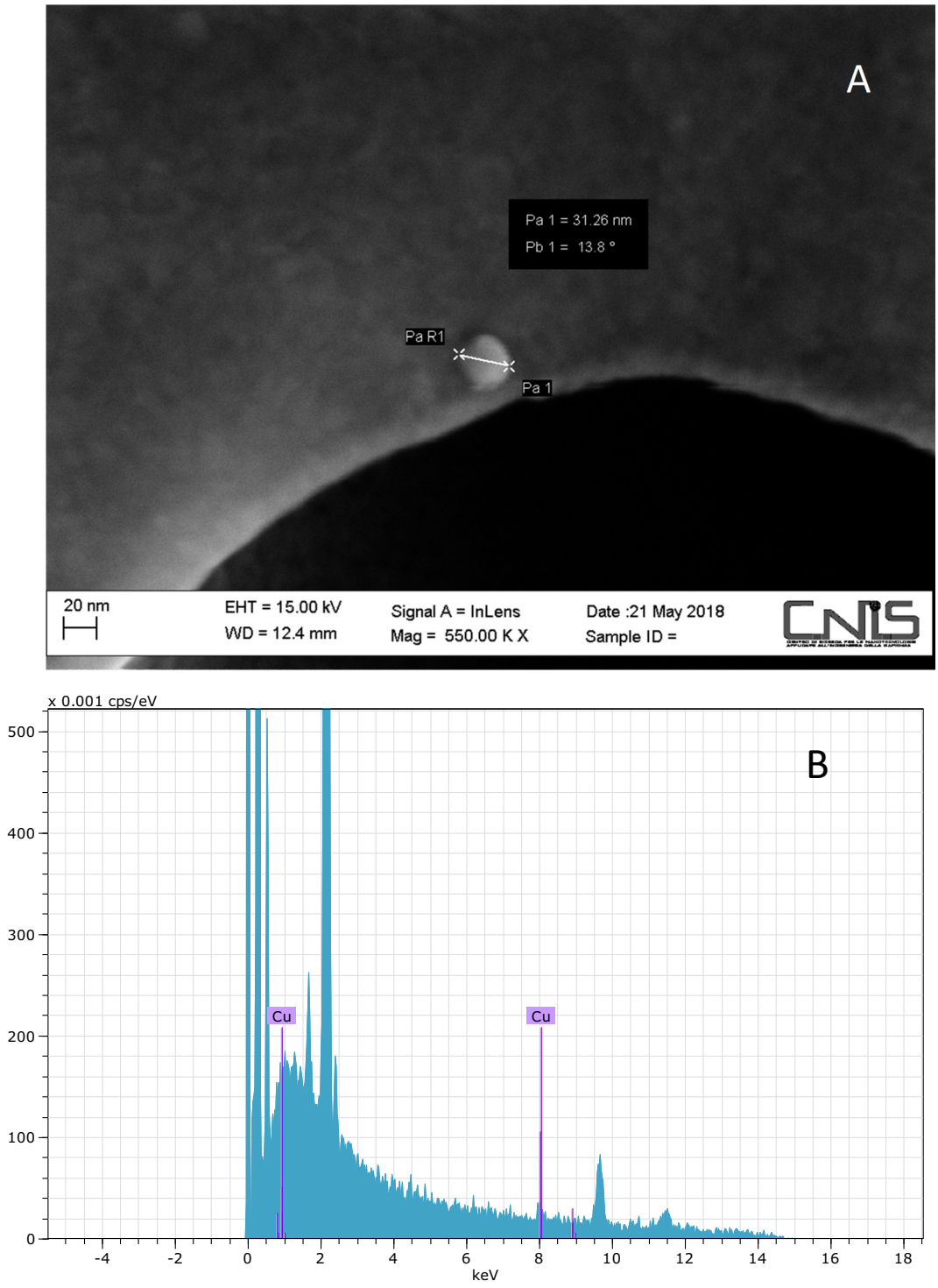

Fig. 4. HR-FESEM micrograph (A) and XEDS microanalysis (B) of nanoparticle emitted by the vacuum cleaner used in DW1.

(6 min, 5 min, 1.5 min, respectively for the vacuum cleaner, the hairdryer and the electric drill), overall 3.8×10^6, 9.0×10^6 and 2.6×10^6 particles ($D_c^{Olf}(t_s)$) were deposited. Median levels of $D^{Olf}(d_i,t)$ for each particle diameter were significantly greater over the period of appliance operation than those estimated before starting the operation (p-value < 0.05) in all cases, with the exception of the highest size fractions that were not appreciably affected by the appliance aerosol emissions.

In terms of particle surface area (Fig. 3d–f), such doses correspond to 61.3, 1.5×10^2, 1.4×10^2 μm^2 after a single respiratory act and to 3.2 $\times 10^3$, 7.4×10^3, 1.2×10^3 μm^2, throughout the time interval of appliance operation ($S_c^{Olf}(t_s)$).

Particle surface area doses represent an important piece of information because NPs, compared with larger-sized particles of the same chemical composition, can generate higher level of Reactive Oxygen Species (ROS), due to their higher surface area per unit mass and to their surface reactivity (Oberdörster et al., 2005). ROS generation has been addressed as the main feature explaining toxic effects of inhaled NPs (Nel et al., 2006), such as DNA damage, unregulated cell signaling,

changes in cell motility, citotoxicity, apoptosis and cancer initiation and promotion (Nel et al., 2006; Xia et al., 2008; Zhu et al., 2013).

The doses reported here represent a small fraction, respectively 0.51%, 0.50% and 0.57%, in terms of particle number metric ($D_c^{Olf}(t_s)$), and 0.15%, 0.27% and 0.43%, in terms of particle surface area metric ($S_c^{Olf}(t_s)$), of the doses deposited in the head region after the same operation time (respectively 7.5×10^8, 1.8×10^9, 4.6×10^8 particles and 2.1×10^6, 2.7×10^6, 2.7×10^5 μm^2, respectively) (Manigrasso et al., 2018). Nonetheless, they are toxicologically relevant, due to their possible translocation to brain (Oberdörster et al., 2005). On this point, Fig. 3g–i compare the number size distribution of the total amount of particle deposited on the olfactory bulb after the appliance operation, $D_c^{Olf}(d_i,t_s)$ (continuous line) with the relevant doses due to the inhalation of background indoor aerosol concentration for the same time interval (dotted line). Bimodal size distributions with modes in between 9 and 11 nm and at 16.5 nm were observed well above the relevant background ones. The histogram in the same figure represents the average value of the frequencies of the magnetite NPs retrieved by Maher et al. (2016) in brain tissue samples, as a function of the longest and of the shortest particle diameters. The authors hypothesized that such NPs may have

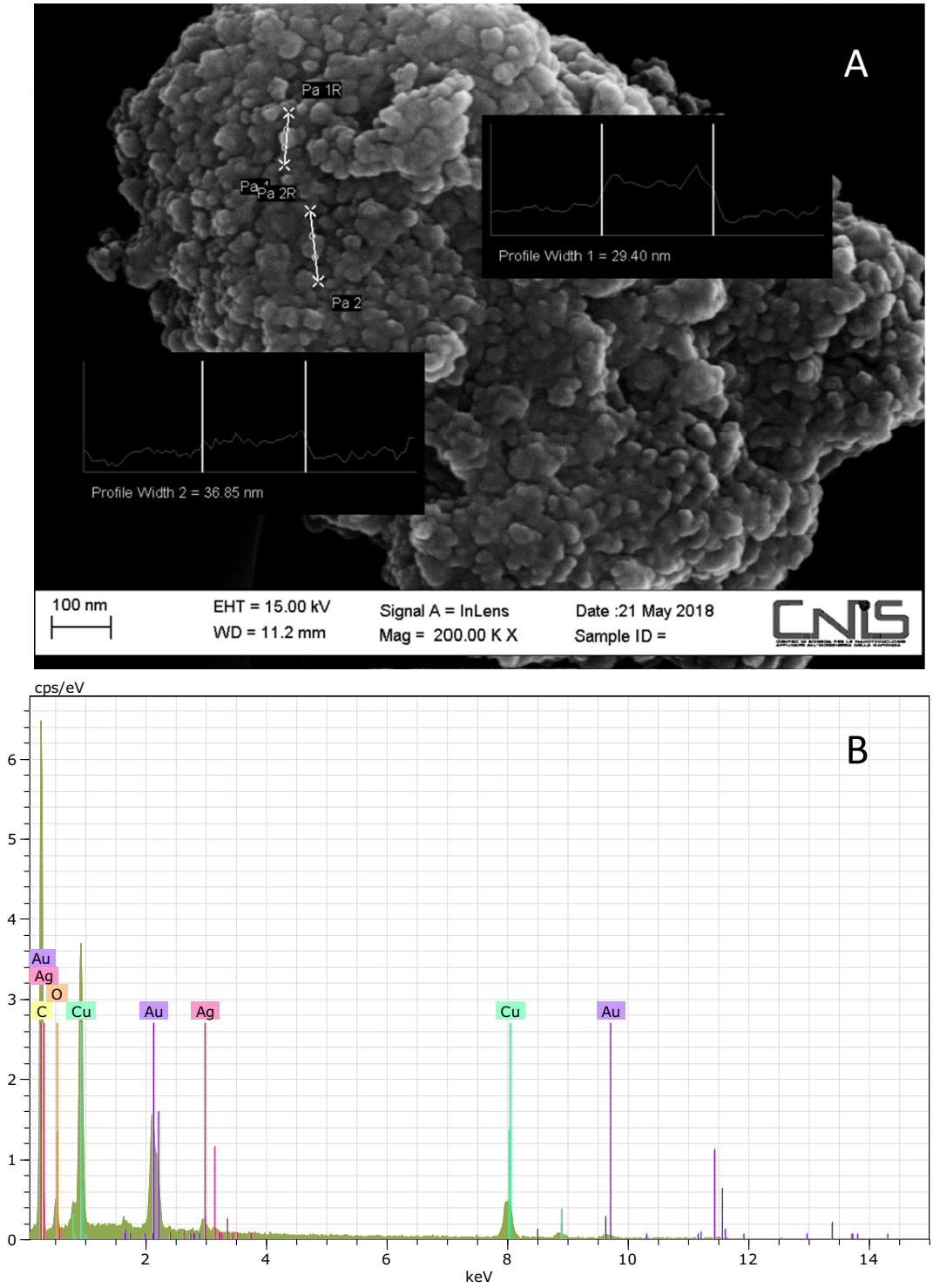

Fig. 5. HR-FESEM micrograph (A) and XEDS microanalysis (B) of a cluster of nanoparticles emitted by the vacuum cleaner used in DW1.

reached the brain directly through the olfactory bulb. The dimensions of these particles are almost the same of those deposited on the olfactory bulb, as estimated in this work. Their elimination, once they have reached the brain, has been reported to possibly proceed by means of the cerebrospinal fluid (CSF) through its connections to the nasal lymphatic system and to the blood circulation (Czerniawska, 1970; Oberdörster et al., 2009; Segal, 2000). More recently, Louveau et al. (2015) have discovered the existence of a meningeal lymphatic system that may represent a further route for CSF to leave the central nervous system.

Health concerns arise due to the role recognized to redox-active metals, such as manganese (Michalke and Fernsebner, 2014; Flynn and Susi, 2009; Santos et al., 2012), iron (Khan et al., 2006; Everett et al., 2018) and Cu (Huang et al., 1999a, 1999b; Fahmy and Cormier, 2009; Tabner et al., 2011) in neurodegenerative diseases, due to their ability to produce ROS. In particular, hot spot Cu and zinc, at higher concentrations than calcium and iron, have been observed, with high spatial correlation, in the amyloid β plaques present in Alzheimer's disease brain tissue samples (Miller et al. 2006). As to the persistence of metal NPs in brain, no much data are available. However, low elimination rates are expected for insoluble NPs, considering also that their metabolic degradation is not envisaged (Geraets et al., 2014). For instance, Geraets et al. (2014) reported half-lives of titanium dioxide NPs in the range 28–650 days, depending on the TiO_2 particles and on the organ investigated. Specifically, as regards Cu NPs solubility, Wongrakpanich et al. (2016) reported that 50% dissolution of 4 nm Cu oxide NPs in RPMI-1640 media at 37 °C occurred over 1 h period, whereas 24 nm NPs took longer (over 24 h). The same authors showed that 24 nm CuO NPs elicit higher cytotoxicity and higher intracellular and mitochondrial ROS production than 4 nm CuO NPs. The authors argued that the 4 nm NP cytotoxicity proceeds through a pathway initiated by the extracellular release of Cu^{2+}, whereas for 24 nm CuO NPs, it seems to be due to the greater intracellular and mitochondria ROS production resulting for the more efficient intracellular access. Therefore, in terms of health effects, both the solubility and the size of Cu NPs are relevant. Moreover, the insoluble form is expected to be biopersistent and to undergo tissue accumulation following repeated exposures.

On this basis, it is relevant both to assess the size together with the metal composition of the NPs released by these appliances and to ascertain the copper indoor contamination, making distinction between its soluble and insoluble fractions, as discussed in the next sessions.

3.2. HR-FESEM characterization

HR-FESEM observation and XEDS microanalyses were performed on filters after sampling of the aerosol emitted from appliances operated by brush electric motors, in order to obtain a qualitative description of individual particle morphology and elemental composition. Figs. 4 and 5 refer to aerosol sampled from the brush electric motor vacuum cleaner used at DW1. They are representative of what has been observed also for the other electric appliances as well (data not shown). Different morphologies of particles were observed. In particular, they were present both as single NPs (20–40 nm) (Fig. 4A) and aggregated in clusters (Fig. 5A). The NP diameters were assumed as the same of the equivalent spherical cross sectional area (Reid et al., 2003; Kandler et al., 2007; Choël et al., 2007) measured by means of HR-FESEM. It is worth observing that also particles of lower sizes (about 10 nm) have been observed, but due to their small dimensions HR-FESEM images were blurred and XEDS microanalysis was not possible to perform (Fig. 6).

In Figs. 4B and 5B spectra from XEDS microanalysis were reported and the presence of copper particles was confirmed for all the NPs found. In particular, Fig. 5B shows the presence of oxygen, suggesting the possibility that Cu is present in the form of an oxide (CuO NPs). As reported in literature (Jeong et al., 2008), Cu NPs easily get oxidized and form particle-particle junctions when heat-treated at high temperature. It should be considered that also the polycarbonate filter may contribute to the oxygen signal, even if such eventuality seems unlike because the XEDS spectrum has been acquired on a particle of large size (1–2 μm). Moreover, the presence of Ag NPs (Fig. 5B) may favor the formation of Cu NPs as aggregates or agglomerates (Fig. 5A), even of large size, through some weak bonds between adjacent particles

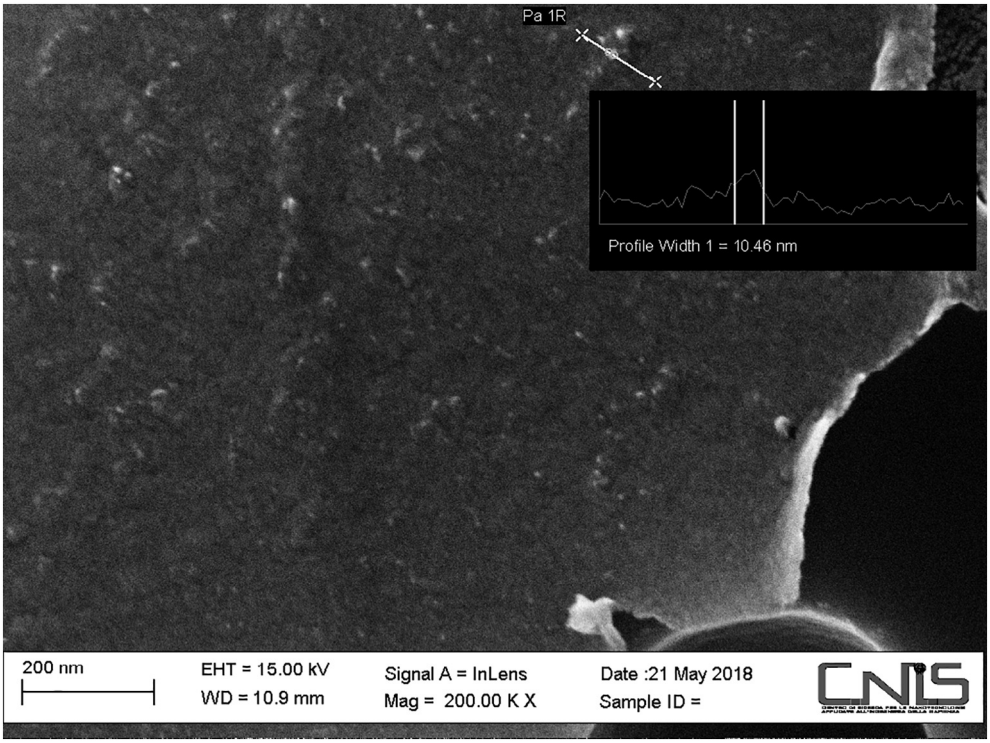

Fig. 6. HR-FESEM micrograph evidencing the presence of NPs of about 10 nm.

(Li et al., 2017). Generally, silver-coated copper powders are used wherever high conductivity (electrical and thermal) is required. In fact, the electrical conductivity of pure Cu is typically deteriorated at elevated temperatures due to oxidation and formation of non-conductive oxides on the surface (J. Li et al., 2016). Instead, the use of Cu together with Ag shows a considerably high electrical conductivity and a high oxidation resistance (J. Li et al., 2016; Li et al., 2017). From the spectrum shown in Fig. 5B, it was possible to highlight the presence of other elements such as Au and C. The presence of Au is due to the treatment of gilding of the filter, necessary for the HR-FESEM XEDS analysis, while C may arise from graphite electrodes of the brush electric motors as well as from grease or lubricant from the motor, or else may also come from the polycarbonate membranes.

Our observations on Cu particles emitted by brush electric motors are in agreement with the findings of Szymczak et al. (2007), who studied the aerosol emissions of a professional vacuum cleaner. Using a MOUDI impactor, they measured broad Cu mass size distributions with modes of about 1–2 μm. Observing that the mass size distribution displayed a higher value for the backup filter than for the lower impactor stage, the authors inferred that a remarkable contribution of Cu NPs was also present. The abundant emission of Cu NPs in the emissions of such appliances is confirmed by the HR-FESEM reported in the present study, and by the highly time resolved aerosol number size distributions reported in a previous study (Manigrasso et al., 2017). Moreover, for the first time, this study shows the relevance of such NPs in terms of the related doses deposited on the olfactory bulb.

The data reported in this paragraph refer to observation of aerosol emitted throughout a few minute operation time interval. A further step forward is to assess in real indoor environments how protracted in time the general population exposure to such NPs is (Section 3.3).

3.3. Cu levels in real scenarios indoor environments

In outdoor environments, Cu is considered as a reliable tracer of the non-combustive contribution to PM due to vehicular traffic. Its concentration in PM_{10} at urban sites is generally very highly correlated to that of Sb, as they share a common prevalent source: antimony trisulphide and Cu are in fact present at high concentration in most brake pad formulations (Pakkanen et al., 2001, Canepari et al., 2010b; Grigoratos and Martini, 2015).

Fig. 7 shows the total Cu and Sb concentrations together with the PM_{10} levels measured throughout one year period in the indoor and outdoor environments at DW1 and DW2 dwellings, where a vacuum cleaner operated by brush and a vacuum cleaner brushless electric motors were respectively used. At both the considered sites, outdoor PM_{10} concentrations (Fig. 7C and F) were higher during the winter season. Terni city is located in an intra-mountain depression and its peculiar geomorphological characteristics cause, especially during the winter, severe episodes of atmospheric stability, which favor the accumulation of air pollutants (Ferrero et al., 2012; Massimi et al., 2017). Seasonal trend of the outdoor Cu and Sb concentrations (Fig. 7A, B, D and E) was less pronounced because during summer the low humidity favors the resuspension of road dust. Furthermore, outdoor PM_{10} concentrations were slightly higher at the DW1 site (brush), more influenced by vehicular traffic than DW2 site (brushless). For the same reason, outdoor concentrations of Cu and Sb were generally higher at DW1 that at DW2. As shown in Fig. 8, outdoor concentrations of Cu and Sb are well correlated at both sites, further confirming the relevance of traffic as the main shared source of both elements. It is worth noting that the ratio Cu/Sb was of about 10, much higher than the value (about 4.5) reported in literature as diagnostic of brake pads contribution to PM (Grigoratos and Martini, 2015). This was probably due to the progressive diffusion in recent years of antimony-free brake pads (Martinez and Echeberria, 2016).

Indoor concentrations of PM_{10} and of Sb were always significantly lower than indoor concentrations, both at DW1 and DW2 sites. The same happened for Cu concentrations measured at DW2 site (Fig. 7D), whereas the reverse situation was observed at DW1 (Fig. 7A) site. Linear regression analysis of Sb vs Cu indoor concentration at DW2 (brushless vacuum cleaner used) still maintains a good correlation (Fig. 8), denoting that infiltration from outside of traffic-related particles was the main source of these two elements. At DW1 site (brush electric motor vacuum cleaner used), Sb and Cu were instead well correlated only outdoor, whereas they were totally uncorrelated indoor. These results clearly indicate the presence of a relevant Cu source in the DW1 indoor environment (indoor Cu levels higher than outdoor), very likely associated to the use of brush electric motor.

Descriptive statistic for indoor and outdoor Cu, Sb and PM_{10} concentration in the two dwellings are reported in Table 2. It is important to note that mean indoor Cu concentration resulted more than two-fold higher than outdoor at DW1 (p-value < 0.001). These findings demonstrate that the contribute from the vacuum cleaner operated by brush motor to the indoor Cu concentration at DW1 was very relevant and significantly increased the exposure to Cu of inhabitants during all the year.

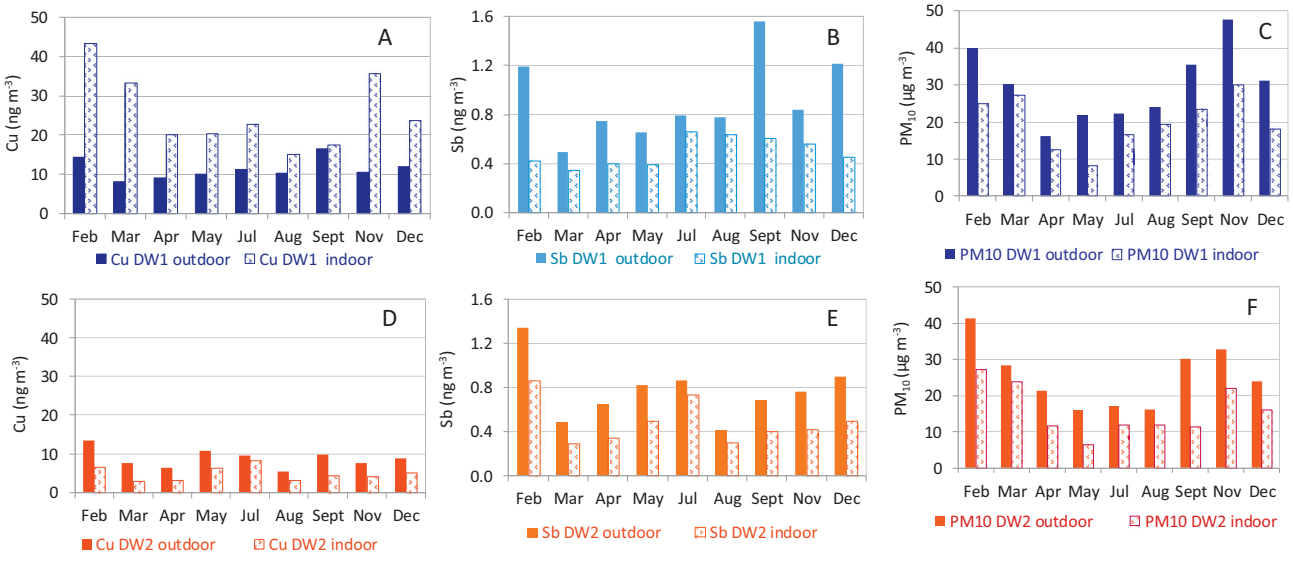

Fig. 7. PM_{10}, Cu and Sb concentration measured indoor and outdoor for DW1 (brush vacuum cleaner - A–C) and DW2 (brushless vacuum cleaner - D–F) dwellings throughout one-year period (9 aerosol samples).

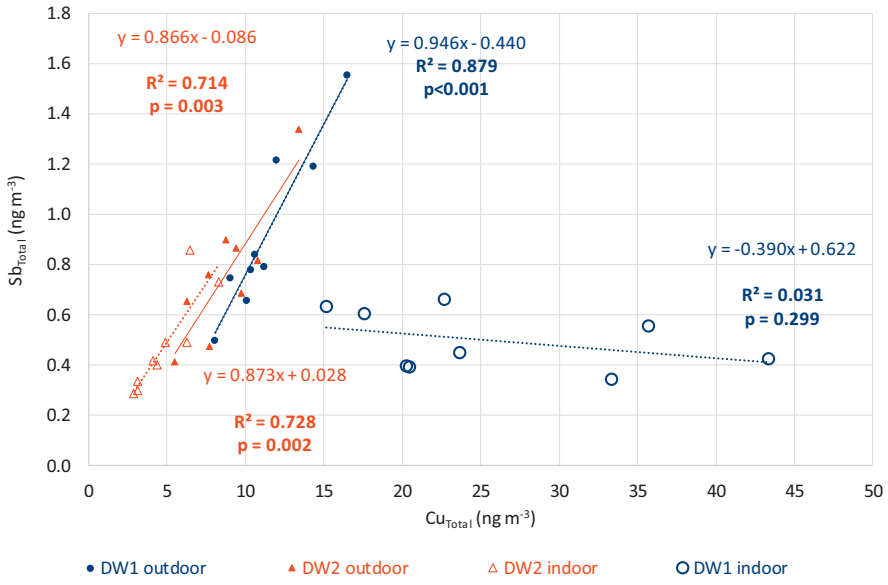

Fig. 8. Relationship between Cu and Sb concentrations measured indoor and outdoor for DW1 (brush vacuum cleaner) and DW2 (brushless vacuum cleaner) dwellings throughout one-year period (9 aerosol samples).

Table 2
Mean levels of PM_{10}, Cu and Sb found indoor and outdoor for DW1 and DW2 dwellings throughout one-year period (9 aerosol samples).

Electric motor	Pollutant	In/out	Mean	SD	p-Value
Brush (DW1)	PM_{10}	Out	29.87	9.93	0.0044
		In	20.86	7.41	
	Cu	Out	11.33	2.62	<0.001
		In	25.77	9.47	
	Sb	Out	0.92	0.33	0.002
		In	0.50	0.12	
Brushless (DW2)	PM_{10}	Out	25.19	8.72	0.023
		In	15.81	6.99	
	Cu	Out	8.80	2.42	0.001
		In	4.85	1.84	
	Sb	Out	0.77	0.27	0.020
		In	0.48	0.20	

Fig. 9 shows the % contribution of the Cu soluble fraction to the total concentration. Similar percentages are observed both indoor and outdoor at DW2 site and outdoor at DW1 site. On the contrary, significantly lower values were measured indoor at DW1 site, suggesting that the indoor Cu emission throughout the whole year monitored brought about an important contribution of insoluble Cu particles. It is worth observing

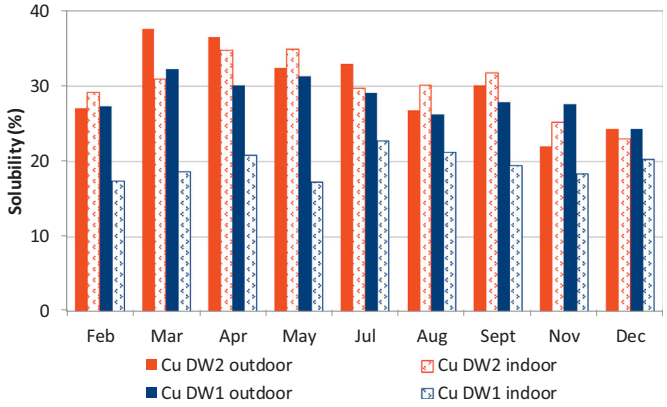

Fig. 9. Percentage of Cu solubility for indoor and outdoor aerosol samples collected in DW1 (brush vacuum cleaner) and DW2 (brushless vacuum cleaner) dwellings throughout one-year period (9 aerosol samples).

that insoluble NPs are more biopersistent and thus susceptible to undergo tissue accumulation. ANOVA test with Bonferroni post-hoc tests confirm that the percentages of the Cu soluble fraction recovered indoor at DW1 site were significantly different from all the other sets of measurements (p-values < 0.001 in all cases).

4. Conclusions

The data discussed show that 10^6–10^7 NPs deposit on the olfactory bulb throughout the use of appliance operated by brush electric motors (operation time 1.5–6 min). The main contribution arises from NPs of the same dimensions of those found by other authors in brain tissue samples. The health relevance of such NPs is not only due to their possible translocation to brain, but also to their chemical composition. As confirmed by HR-FESEM observations, they almost invariably contained Cu, an element addressed by many studies to play an important role on the onset of neurodegenerative diseases. To ascertain to what extent the general population is exposed, about 1-month averaged PM_{10} samples were collected in private dwellings throughout a year, and the relevant Cu content was determined. It was demonstrated that the operation of this kind of appliances caused indoor Cu concentrations more than two–fold higher than in outdoor, with a predominant contribution of the Cu insoluble fraction. Moreover, the exposure pattern is chronic. Cu NPs, for the amount they provide to the insoluble fraction, has the potential of undergoing harmful tissue accumulation.

The electric appliances considered in this study are widely diffused and are currently used in indoor environments with daily, and in some case more than daily, frequency. Every individual is directly exposed while utilizing them and indirectly, by simply residing in the environments where they have been used.

Funding

This research did not receive any specific grant from funding agencies in the public, commercial, or not-for-profit sectors.

Acknowledgments

The authors gratefully thank Mr. R. Palomba for his helpful support in carrying out the measurements and to Dr. M. Ristorini for her essential help in PM_{10} samplings. Thanks are also due to Dr. F. Mura for his

kind assistance in HR-FESEM micrograph and XEDS microanalysis acquisition, and to ARA for MPPD version 3.01. This study was carried out as a part of the research program 2016–2018 of the National Institute for Insurance Against Accidents at Work (INAIL), Italy and of the framework agreement between INAIL and La Sapienza University of Rome; Italy.

References

Anderson, J.O., Thundiyil, J.G., Stolbach, A., 2012. Clearing the air: a review of the effects of particulate matter air pollution on human health. J. Med. Toxicol. 8, 166–175. https://doi.org/10.1007/s13181-011-0203-1.

Asgharian, B., Hofmann, W., Bergmann, R., 2001. Particle deposition in a multiple-path model of the human lung. Aerosol Sci. Technol. 34, 332–339. https://doi.org/10.1080/02786820119122.

Astolfi, M.L., Marconi, E., Protano, C., Vitali, M., Schiavi, E., Mastromarino, P., Canepari, S., 2018. Optimization and validation of a fast digestion method for the determination of major and trace elements in breast milk by ICP-MS. Anal. Chim. Acta https://doi.org/10.1016/j.aca.2018.07.037 in press.

Bau, S., Witschger, O., Gensdarmes, F., Thomas, D., Borra, J.-P., 2010. Electrical properties of airborne nanoparticles produced by a commercial spark-discharge generator. J. Nanopart. Res. 12, 1989–1995. https://doi.org/10.1007/s11051-010-9856-y.

Brauer, M., Koutrakis, P., Spengler, J.D., 1989. Personal exposures to acidic aerosols and gases. Environ. Sci. Technol. 23, 1408–1412. https://doi.org/10.1021/es00069a013.

Burris, H.H., Baccarelli, A.A., 2017. Air pollution and in utero programming of poor fetal growth. Epigenomics 9, 213–216. https://doi.org/10.2217/epi-2017-0008.

CalEPA, 2004. Indoor Air Pollution in California. Air Resources Board, California Environmental Protection Agency, Sacramento, CA.

Canepari, S., Cardarelli, E., Giuliano, A., Pietrodangelo, A., 2006a. Determination of metals, metalloids and non-volatile ions in airborne particulate matter by a new two-step sequential leaching procedure. Part A: experimental design and optimisation. Talanta 69, 581–587. https://doi.org/10.1016/j.talanta.2005.10.024.

Canepari, S., Cardarelli, E., Pietrodangelo, A., Strincone, M., 2006b. Determination of metals, metalloids and non-volatile ions in airborne particulate matter by a new two-step sequential leaching procedure. Part B: validation on equivalent real samples. Talanta 69, 588–595. https://doi.org/10.1016/j.talanta.2005.10.023.

Canepari, S., Perrino, C., Astolfi, M.L., Catrambone, M., Perret, D., 2009. Determination of soluble ions and elements in ambient air suspended particulate matter: inter-technique comparison of XRF, IC and ICP for sample-by-sample quality control. Talanta 77, 1821–1829. https://doi.org/10.1016/j.talanta.2008.10.029.

Canepari, S., Marconi, E., Astolfi, M.L., Perrino, C., 2010a. Relevance of Sb(III), Sb(V), and Sb-containing nano-particles in urban atmospheric particulate matter. Anal. Bioanal. Chem. 397, 2533–2542. https://doi.org/10.1007/s00216-010-3818-1.

Canepari, S., Astolfi, M.L., Moretti, S., Curini, R., 2010b. Comparison of extracting solutions for elemental fractionation in airborne particulate matter. Talanta 82, 834–844. https://doi.org/10.1016/j.talanta.2010.05.068.

Castellano, P., Canepari, S., Ferrante, R., L'Episcopo, N., 2012. Multiparametric approach for an exemplary study of laser printer emissions. J. Environ. Monit. 14, 446–454. https://doi.org/10.1039/c2em10696e.

Charvet, A., Bau, S., Paez Coy, N.E., Bemer, D., Thomas, D., 2014. Characterizing the effective density and primary particle diameter of airborne nanoparticles produced by spark discharge using mobility and mass measurements (tandem DMA/APM). J. Nanopart. Res. 16, 2418. https://doi.org/10.1007/s11051-014-2418-y.

Choël, M., Deboudt, K., Flament, P., 2007. Evaluation of quantitative procedures for X-ray microanalysis of environmental particles. Microsc. Res. Tech. 70, 996–1002. https://doi.org/10.1002/jemt.20510, 2007.

Czerniawska, A., 1970. Experimental investigations on the penetration of ^{198}Au from nasal mucous membrane into cerebrospinal fluid. Acta Otolaryngol. 70, 58–61.

Darbre, P.D., 2018. Overview of air pollution and endocrine disorders. Int. J. Gen. Med. 11, 191–207. https://doi.org/10.2147/IJGM.S102230.

Drago, G., Perrino, C., Canepari, S., Ruggieri, S., L'Abbate, L., Longo, V., Colombo, P., Frasca, D., Balzan, M., Cuttitta, G., Scaccianoce, G., Piva, G., Buccheri, S., Melis, M., Viegi, G., Cibella, F., 2018. Relationship between domestic smoking and metals and rare earth elements concentration in indoor $PM_{2.5}$. Environ. Res. 165, 71–80. https://doi.org/10.1016/j.envres.2018.03.026.

Everett, J., Collingwood, J.F., Tjendana-Tjhin, V., Brooks, J., Lermyte, F., Plascencia-Villa, G., Hands-Portman, I., Dobson, J., Perry, G., Telling, N.D., 2018. Nanoscale synchrotron X-ray speciation of iron and calcium compounds in amyloid plaque cores from Alzheimer's disease subjects. Nanoscale https://doi.org/10.1039/c7nr06794a.

Fahmy, B., Cormier, S.A., 2009. Copper oxide nanoparticles induce oxidative stress and cytotoxicity in airway epithelial cells. Toxicol. in Vitro 23, 1365–1371. https://doi.org/10.1016/j.tiv.2009.08.005.

Ferrero, L., Cappelletti, D., Moroni, B., Sangiorgi, G., Perrone, M.G., Crocchianti, S., Bolzacchini, E., 2012. Wintertime aerosol dynamics and chemical composition across the mixing layer over basin valleys. Atmos. Environ. 56, 143–153. https://doi.org/10.1016/j.atmosenv.2012.03.071.

Flynn, M.R., Susi, P., 2009. Neurological risks associated with manganese exposure from welding operations–a literature review. Int. J. Hyg. Environ. Health 212, 459–469. https://doi.org/10.1016/j.ijheh.2008.12.003.

Frasca, D., Marcoccia, M., Tofful, L., Simonetti, G., Perrino, C., Canepari, S., 2018. Influence of advanced wood-fired appliances for residential heating on indoor air quality. Chemosphere 211, 62–71. https://doi.org/10.1016/j.chemosphere.2018.07.102.

Garcia, G.J., Schroeter, J.D., Kimbell, J.S., 2015. Olfactory deposition of inhaled nanoparticles in humans. Inhal. Toxicol. 27, 394–403. https://doi.org/10.3109/08958378.2015.1066904.

Geraets, L., Oomen, A.G., Krystek, P., Jacobsen, N.R., Wallin, H., Laurentie, M., Verharen, H.W., Brandon, E.F., de Jong, W.H., 2014. Tissue distribution and elimination after oral and intravenous administration of different titanium dioxide nanoparticles in rats. Part Fibre Toxicol. 11, 30. https://doi.org/10.1186/1743-8977-11-30.

Grigoratos, T., Martini, G., 2015. Brake wear particle emissions: a review. Environ. Sci. Pollut. Res. 22, 2491–2504. https://doi.org/10.1007/s11356-014-3696-8.

Hoek, G., Boogaard, H., Knol, A., de Hartog, J., Slottje, P., Ayres, J.G., Borm, P., Brunekreef, B., Donaldson, K., Forastiere, F., Holgate, S., Kreyling, W.G., Nemery, B., Pekkanen, J., Stone, V., Wichmann, H.E., van der Sluijs, J., 2010. Concentration response functions for ultrafine particles and all-cause mortality and hospital admissions: results of a European expert panel elicitation. Environ. Sci. Technol. 44, 476–482. https://doi.org/10.1021/es9021393.

Hsu, D.J., Huang, H.L., Sheu, S.C., 2012. Characteristics of air pollutants and assessment of potential exposure in spa centers during aromatherapy. Environ. Eng. Sci. 29, 79–85. https://doi.org/10.1089/ees.2011.0004.

Huang, X., Atwood, C.S., Hartshorn, M.A., Multhaup, G., Goldstein, L.E., Scarpa, R.C., Cuajungco, M.P., Gray, D.N., Lim, J., Moir, R.D., Tanzi, R.E., Bush, A.I., 1999a. The Aβ peptide of Alzheimer's disease directly produces hydrogen peroxide through metal ion reduction. Biochemist 38, 7609–7616. https://doi.org/10.1021/bi990438f.

Huang, X., Cuajungco, M.P., Atwood, C.S., Hartshorn, M.A., Tyndall, J.D.A., Hanson, G.R., Stokes, K.C., Leopold, M., Multhaup, G., Goldstein, L.E., Scarpa, R.C., Saunders, A.J., Lim, J., Moir, R.D., Glabe, C., Bowden, E.F., Masters, C.L., Fairlie, D.P., Tanzi, R.E., Busha, A.I., 1999b. Cu(II) potentiation of Alzheimer Aβ neurotoxicity. Correlation with cell-free hydrogen peroxide production and metal reduction. J. Biol. Chem. 274, 37111–37116.

Huang, H.L., Tsai, T.J., Hsu, N.Y., Lee, C.C., Wu, P.C., Su, H.J., 2012. Effects of essential oils on the formation of formaldehyde and secondary organic aerosols in an aromatherapy environment. Build. Environ. 57, 120–125. https://doi.org/10.1016/j.buildenv.2012.04.020.

Hubal, E.A.C., Sheldon, L.S., Burke, J.M., McCurdy, T.R., Berry, M.R., Rigas, M.L., Zartarian, V.G., Freeman, N.C., 2000. Children's exposure assessment: a review of factors influencing children's exposure, and the data available to characterize and assess that exposure. Environ. Health Perspect. 108, 475–486.

IARC, 2013. IARC: Outdoor air pollution a leading environmental cause of cancer deaths. Available at: https://www.iarc.fr/en/media-centre/iarcnews/pdf/pr221_E.pdf. (last accessed 06 June 2018).

ICRP, 1994. Human respiratory tract model for radiological protection. A report of a task group of the International Commission on Radiological Protection. Ann. ICRP 24, 1–482.

Jeong, C.-H., Evans, G.J., 2009. Inter-comparison of a fastmobility particle sizer and a scanning mobility particle sizer incorporating an ultrafine water based condensation particle counter. Aerosol Sci. Technol. 43, 364–373. https://doi.org/10.1080/02786820802662939.

Jeong, S., Woo, K., Kim, D., Lim, S., Kim, J.S., Shin, H., Xia, Y., Moon, J., 2008. Controlling the thickness of the surface oxide layer on Cu nanoparticles for the fabrication of conductive structures by ink-jet printing. Adv. Funct. Mater. 18, 679–686. https://doi.org/10.1002/adfm.200700902.

Kandler, K., Benker, N., Bundke, U., Cuevas, E., Ebert, M., Knippertz, P., Rodríguez, S., Schütz, L., Weinbruch, S., 2007. Chemical composition and complex refractive index of Saharan mineral dust at Izaˇna, Tenerife (Spain) derived by electron microscopy. Atmos. Environ. 41, 8058–8074.

Khan, A., Dobson, J.P., Exley, C., 2006. Redox cycling of iron by Abeta42. Free Radic. Biol. Med. 40, 557–569. https://doi.org/10.1016/j.freeradbiomed.2005.09.013.

Laussmann, D., Helm, D., 2011. Air change measurements using tracer gases: methods and results. Significance of air change for indoor air quality. In: Mazzeo, M. (Ed.), Chemistry, Emission Control, Radioactive Pollution and Indoor Air Quality. InTech, Rijeka, Croatia, pp. 365–406.

Levesque, S., Surace, M.J., McDonald, J., Block, M.L., 2011. Air pollution & the brain: subchronic diesel exhaust exposure causes neuroinflammation and elevates early markers of neurodegenerative disease. J. Neuroinflammation 8, 105. https://doi.org/10.1186/1742-2094-8-105.

Li, N., Sioutas, C., Cho, A., Schmitz, D., Misra, C., Sempf, J., Wang, M., Oberley, T., Froines, J., Nel, A., 2003. Ultrafine particulate pollutants induce oxidative stress and mitochondrial damage. Environ. Health Perspect. 11, 455–460.

Li, J., Li, Y., Wang, Z., Bian, H., Hou, Y., Wang, F., Xu, G., Liu, B., Liu, Y., 2016. Ultrahigh oxidation resistance and high electrical conductivity in copper-silver powder. Sci. Rep. 6, 39650. https://doi.org/10.1038/srep39650.

Li, X., Yan, C., Patterson, R.F., Zhu, Y., Yao, X., Zhu, Y., Ma, S., Qiu, X., Zhu, T., Mei Zheng, M., 2016. Modeled deposition of fine particles in human airway in Beijing, China. Atmos. Environ. 124, 387–395. https://doi.org/10.13227/j.hjkx.201610040.

Li, W., Hu, D., Li, L., Li, C.-F., Jiu, J., Chen, C., Ishina, T., Sugahara, T., Suganuma, K., 2017. Printable and flexible copper−silver alloy electrodes with high conductivity and ultrahigh oxidation resistance. ACS Appl. Mater. Interfaces 9, 24711–24721. https://doi.org/10.1021/acsami.7b05308.

Liu, J., Fung, D., Jiang, J., Zhu, Y., 2014. Ultrafine particle emissions from essential-oil-based mosquito repellent products. Indoor Air 24, 327–335. https://doi.org/10.1111/ina.12080.

Louveau, A., Smirnov, I., Keyes, T.J., Eccles, J.D., Rouhani, S.J., Peske, J.D., Derecki, N.C., Castle, D., Mandell, J.W., Lee, K.S., Harris, T.H., Kipnis, J., 2015. Structural and functional features of central nervous system lymphatic vessels. Nature 523, 337–341. https://doi.org/10.1038/nature14432.

Maher, B.A., Ahmed, I.A.M., Karloukovski, V., MacLaren, D.A., Foulds, P.G., Allsop, D., Mann, D.M.A., Torres-Jardón, R., Calderon-Garciduenas, L., 2016. Magnetite pollution nanoparticles in the human brain. PNAS 113, 10797–10801. https://doi.org/10.1073/pnas.1605941113.

Manigrasso, M., Avino, P., 2012. Fast evolution of urban ultrafine particles: implications for deposition doses in the human respiratory system. Atmos. Environ. 51, 116–123. https://doi.org/10.1016/j.atmosenv.2012.01.039.
Manigrasso, M., Stabile, L., Avino, P., Buonanno, G., 2013. Influence of measurement frequency on the evaluation of short-term dose of sub-micrometric particles during indoor and outdoor generation events. Atmos. Environ. 67, 130–142. https://doi.org/10.1016/j.atmosenv.2012.10.059.
Manigrasso, M., Guerriero, E., Avino, P., 2015. Ultrafine particles in residential indoors and doses deposited in the human respiratory system. Atmosphere 6, 1444–1461. https://doi.org/10.3390/atmos6101444.
Manigrasso, M., Vitali, M., Protano, C., Avino, P., 2017. Temporal evolution of ultrafine particles and of alveolar deposited surface area from main indoor combustion and non-combustion sources in a model room. Sci. Total Environ. 15, 1015–1026. https://doi.org/10.1016/j.scitotenv.2017.02.048.
Manigrasso, M., Vitali, M., Protano, C., Avino, P., 2018. Ultrafine particles in domestic environments: regional doses deposited in the human respiratory system. Environ. Int. 118, 134–145. https://doi.org/10.1016/j.envint.2018.05.049.
Mannucci, P.M., Harari, S., Martinelli, I., Franchini, M., 2015. Effects on health of air pollution: a narrative review. Intern. Emerg. Med. 10, 657–662. https://doi.org/10.1007/s11739-015-1276-7.
Martinez, A.M., Echeberria, J., 2016. Towards a better understanding of the reaction between metal powders and the solid lubricant Sb2S3 in a low-metallic brake pad at high temperature. Wear 348, 27–42. https://doi.org/10.1016/j.wear.2015.11.014.
Massimi, L., Ristorini, M., Eusebio, M., Florendo, D., Adeyemo, A., Brugnoli, D., Canepari, S., 2017. Monitoring and evaluation of Terni (Central Italy) air quality through spatially resolved analyses. Atmosphere 8, 200. https://doi.org/10.3390/ecas2017-04129.
Michalke, B., Fernsebner, K., 2014. New insights into manganese toxicity and speciation. J. Trace Elem. Med. Biol. 28, 106–116. https://doi.org/10.1016/j.jtemb.2013.08.005.
Miller, L.M., Wang, Q., Telivala, T.P., Smith, R.J., Lanzirotti, A., Miklossy, J., 2006. Synchrotron-based infrared and X-ray imaging shows focalized accumulation of cu and Zn co-localized with beta-amyloid deposits in Alzheimer's disease. J. Struct. Biol. 155, 30–37. https://doi.org/10.1016/j.jsb.2005.09.004.
Morawska, L., Ayoko, G.A., Bae, G.N., Buonanno, G., Chao, C.Y.H., Clifford, S., Fu, S.C., Hänninen, O., He, C., Isaxon, C., Mazaheri, M., Salthammer, T., Waring, M.S., Wierzbicka, A., 2017. Airborne particles in indoor environment of homes, schools, offices and aged care facilities: the main routes of exposure. Environ. Int. 108, 75–83. https://doi.org/10.1016/j.envint.2017.07.025.
Nel, A., Xia, T., Mädler, L., Li, N., 2006. Toxic potential of materials at the nanolevel. Science 311, 622–627. https://doi.org/10.1126/science.1114397.
Noh, J., Sohn, J., Cho, J., Kim, C., Shin, D.C., 2016. YIA 02-02 long-term effects of fine particulate matter exposures on major adverse cardiovascular events. J. Hypertens. 34, e202. https://doi.org/10.1097/01.hjh.0000500437.46224.7e.
Oberdörster, G., Oberdörster, E., Oberdörster, J., 2005. Nanotoxicology: an emerging discipline evolving from studies of ultrafine particles. Environ. Health Perspect. 113, 823–839. https://doi.org/10.1289/ehp.7339.
Oberdörster, G., Elder, A., Rinderknecht, A., 2009. Nanoparticles and the brain: cause for concern? J. Nanosci. Nanotechnol. 9, 4996–5007. https://doi.org/10.1166/jnn.2009.GR02.
Pagano, P., De Zaiacomo, T., Scarcella, E., Bruni, S., Calamosca, M., 1996. Mutagenic activity of total and particle-sized fractions of urban particulate matter. Environ. Sci. Technol. 30, 3512–3516. https://doi.org/10.1021/es960182q.
Pakkanen, T.A., Loukkola, K., Korhonen, C.H., Aurela, M., Mäkelä, T., Hillamo, R.E., Aarnio, P., Koskentalo, T., Kousa, A., Maenhaut, W., 2001. Sources and chemical composition of atmospheric fine and coarse particles in the Helsinki area. Atmos. Environ. 35, 5381–5391. https://doi.org/10.1016/S1352-2310(01)00307-7.
Protano, C., Manigrasso, M., Avino, P., Sernia, S., Vitali, M., 2016. Second-hand smoke exposure generated by new electronic devices (IQOS® and e-cigs) and traditional cigarettes: submicron particle behaviour in human respiratory system. Ann. Ig. 28, 109–112. https://doi.org/10.7416/ai.2016.2089.
Protano, C., Manigrasso, M., Avino, P., Vitali, M., 2017. Second-hand smoke generated by combustion and electronic smoking devices used in real scenarios: ultrafine particle pollution and age-related dose assessment. Environ. Int. 107, 190–195. https://doi.org/10.1016/j.envint.2017.07.014.
Reid, J.S., Jonsson, H.H., Maring, H.B., Smirnov, A., Savoie, D.L., Cliff, S.S., Reid, E.A., Livingston, J.M., Meier, M.M., Dubovik, O., Tsay, S.C., 2003. Comparison of size and morphological measurements of coarse mode dust particles from Africa. J. Geophys. Res. 108, 8593. https://doi.org/10.1029/2002JD002485.
Roth, C., Ferron, G.A., Karg, E., Lentner, B., Schumann, G., Takenaka, S., Heyder, J., 2004. Generation of ultrafine particles by spark discharging. Aerosol Sci. Technol. 38, 228–235. https://doi.org/10.1080/02786820490247632.
Santos, D., Milatovic, D., Andrade, V., Batoreu, M.C., Aschner, M., Marreilha dos Santos, A.P., 2012. The inhibitory effect of manganese on acetylcholinesterase activity enhances oxidative stress and neuroinflammation in the rat brain. Toxicology 292, 90–98. https://doi.org/10.1016/j.tox.2011.11.017.
Sarwar, G., Olson, D.A., Corsi, R.L., Weschler, C.J., 2004. Indoor fine particles: the role of terpene emissions from consumer products. J. Air Waste Manage. Assoc. 54, 367–377. https://doi.org/10.1080/10473289.2004.10470910.
Scungio, M., Vitanza, T., Stabile, L., Buonanno, G., Morawska, L., 2017. Characterization of particle emission from laser printers. Sci. Total Environ. 586, 623–630. https://doi.org/10.1016/j.scitotenv.2017.02.030.
Segal, M.B., 2000. The choroid plexuses and the barriers between the blood and the cerebrospinal fluid. Cell. Mol. Neurobiol. 20, 183–196.
Śmiełowska, M., Marć, M., Zabiegała, B., 2017. Indoor air quality in public utility environments-a review. Environ. Sci. Pollut. Res. 24, 11166–11176. https://doi.org/10.1007/s11356-017-8567-7.
Stabile, L., Buonanno, G., Avino, P., Frattolillo, A., Guerriero, E., 2018. Indoor exposure to particles emitted by biomass-burning heating systems and evaluation of dose and lung cancer risk received by population. Environ. Pollut. 235, 65–73. https://doi.org/10.1016/j.envpol.2017.12.055.
Szymczak, W., Menzel, N., Keck, L., 2007. Emission of ultrafine copper particles by universal motors controlled by phase angle modulation. J. Aerosol. Sci. 38, 520–531. https://doi.org/10.1016/j.jaerosci.2007.03.002.
Tabner, B.J., Mayes, J., Allsop, D., 2011. Hypothesis: soluble Aβ oligomers in association with redox-active metal ions are the optimal generators of reactive oxygen species in Alzheimer's disease. Int. J. Alzheimers Dis. 546380. https://doi.org/10.4061/2011/546380.
TSI Particle Technology, 2015. Available online. http://www.tsi.com/Fast-Mobility-Particle-Sizer-Spectrometer-3091/# (last accessed on 13 June 2018).
Veleminsky Jr., M.-, Hanzl, M., Sram, R.J., 2016. The impact of air pollution in the southern Bohemia region on fetuses and newborns. Neuro Endocrinol. Lett. 37 (Suppl. 2), 52–57.
Wang, Y., Xiong, L., Tang, M., 2017. Toxicity of inhaled particulate matter on the central nervous system: neuroinflammation, neuropsychological effects and neurodegenerative disease. J. Appl. Toxicol. 37, 644–667. https://doi.org/10.1002/jat.3451.
Westergaard, N., Gehring, U., Slama, R., Pedersen, M., 2017. Ambient air pollution and low birth weight - are some women more vulnerable than others? Environ. Int. 104, 146–154. https://doi.org/10.1016/j.envint.2017.03.026.
WHO, 2018. Air Pollution. WHO Global Ambient Air Quality Database (Update 2018). Available at: http://www.who.int/airpollution/data/cities/en/ (last accessed 06 June 2018).
Wongrakpanich, A., Mudunkotuwa, I.A., Geary, S.M., Morris, A.S., Mapuskar, K.A., Spitz, D.R., Grassian, V.H., Salem, A.K., 2016. Size-dependent cytotoxicity of copper oxide nanoparticles in lung epithelial cells. Environ. Sci. Nano. 3, 365–374. https://doi.org/10.1039/C5EN00271K.
Xia, T., Kovochich, M., Liong, M., Mädler, L., Gilbert, B., Shi, H., Yeh, J.I., Zink, J.I., Nel, A.E., 2008. Comparison of the mechanism of toxicity of zinc oxide and cerium oxide nanoparticles based on dissolution and oxidative stress properties. ACS Nano 2, 2121–2134. https://doi.org/10.1021/nn800511k.
Zhu, X., Hondroulis, E., Liu, W., Li, C.Z., 2013. Biosensing approaches for rapid genotoxicity and cytotoxicity assays upon nanomaterial exposure. Small 9, 1821–1830. https://doi.org/10.1002/smll.201201593.